Two stages of accelerated exhumation in the middle reach of the Yarlung River, southern Tibet since the mid-Miocene

Jin-Gen Dai[1]*, Matthew Fox[2], Xu Han[1], Marissa M. Tremblay[3], Shi-Ying Xu[1], David L. Shuster[4,5], Bo-Rong Liu[1], Jiawei Zhang[6], Cheng-Shan Wang[1,7]

[1]School of Earth Sciences and Resources, Research Center for Tibetan Plateau Geology, China University of Geosciences, Beijing 100083, China.

[2] Department of Earth Science, University College London, Gower Street, London, UK.

[3] Department of Earth, Atmospheric, and Planetary Sciences, Purdue University, West Lafayette, Indiana, 47907, USA.

[4] Department of Earth and Planetary Science, University of California, Berkeley, CA94720, USA.

[5] Berkeley Geochronology Center, 2455 Ridge Road, Berkeley, CA94709, USA.

[6] State Key Laboratory of Earthquake Dynamics, Institute of Geology, China Earthquake Administration, Beijing, China.

[7] State Key Laboratory of Biogeology and Environmental Geology, China University of Geosciences, Beijing 100083, China.

Corresponding author: Jin-Gen Dai (djgtibet@163.com)

Key Points:

- Two stages of accelerated exhumation occurred in different parts of the middle reach of the Yarlung River.
- Mid-Miocene rapid exhumation of wide valley and its tributaries was related to enhanced precipitation and extension.
- Pliocene-Pleistocene accelerated exhumation of gorges was associated with north-south normal faulting.

This article has been accepted for publication and undergone full peer review but has not been through the copyediting, typesetting, pagination and proofreading process, which may lead to differences between this version and the Version of Record. Please cite this article as doi: 10.1029/2020TC006618.

Abstract

Climate change and tectonic activity through erosion control Earth's topography, much of which is shaped by river incision. The Yarlung River has dissected the Indian-Asian Collision Zone, and is one of the Earth's largest rivers. However, its erosion rate history and how it interacts with regional tectonics remain ambiguous. Here we apply low-temperature thermochronometry and thermal-kinematic models for bedrock samples from the Yarlung River. Our analysis reveals two stages of relatively fast exhumation occurred in different parts of the middle reach of the Yarlung River followed by remarkedly slow exhumation rate. First, a mid-Miocene period (15-9 Ma) of rapid exhumation occurred along much of the Yarlung River, including within wide portions of the valley and its tributaries. This period of rapid exhumation coincides with the stage of high precipitation rates recorded in the Asian marginal basins and the timing of the east-west extensional faults. In combination with extensional faults, the enhanced precipitation due to the onset of Asian monsoon would increase river discharge and thus accelerate mid-Miocene exhumation rates. Second, a Pliocene-Pleistocene (5-2 Ma) period of accelerated exhumation limited to gorges occurred in response to north-south normal faulting, implying local tectonics as a first-order control. Our results highlight roles of climatic and tectonic processes in shaping fluvial topography and how these change with time.

1 Introduction

Orogenic topography results from the complex processes imposed by climate, tectonics and their feedbacks mainly through river incision (e.g., Champagnac et al., 2012; Whipple, 2004). In this context, fluvial topography and exhumation rate histories can provide an archive of climatic (e.g., Bender et al., 2020) and tectonic (e.g., Schildgen et al., 2007) changes with time. As fluvial topography evolves over geological time, the control it exerts on erosion would also change with time (e.g., Champagnac et al., 2012), but how the control changes through time remains ambiguous. The Tibetan Plateau is the highest plateau on Earth and is characterized by high topographic relief at its margins (Montgomery and Brandon, 2002; Yin, 2006) formed through river incision (Figure 1) and these rivers are expected to be very sensitive to climate and tectonic changes (e.g., Nie et al., 2018). There are several large river drainages including the Yangtze, Mekong, Salween and Yarlung across the southern and southeastern Tibetan Plateau and Himalayas (Figure 1). Their unusual geometries and topographies have been considered to be the result of tectonic deformation and drainage reorganization (e.g., Wang et al, 2014b; Zhang et al., 2019; Fox et al., 2020), as well as climate change (e.g., Nie et al., 2018). Therefore, rivers in the Tibetan Plateau and the Himalayas are natural laboratories to investigate the complex links amongst tectonics, climate, surface process and drainage reorganization.

The west-to-east flowing Yarlung River, located within the Indian-Asian Collision Zone (IACZ, including the Gangdese arc, the Yarlung Zangbo Suture Zone, and the Tethyan Himalayas), is one of the largest rivers that flows from the Tibetan Plateau (Figures 1 and 2). Its source is high in southern Tibet and the Yarlung River cuts through the eastern syntaxis before flowing through Siang River into the Brahmaputra River. Provenance studies from the Oligocene to Pliocene sediments in the Indo-Burma Range (IBR) peripheral basin of the ancestral Brahmaputra delta reveal an increase in the proportion of Gangdese arc materials at the expense of Himalayan sources at around 12 Ma. This suggests enhanced erosion of the Yarlung-Brahmaputra river following the mid-Miocene onset of the Indian Monsoon (Betka et al., 2019). However, the exhumation histories and their controls of the middle reach of the Yarlung River which mainly cuts through the southern part of the Gangdese arc remain unclear.

At least five knickpoints have developed along the Yarlung River (e.g., Zhang et al., 2016), with narrow gorges separated by braided valleys (Zhang, 1998). The Yarlung Gorge is the steepest knickpoint and one of the deepest canyons on Earth. The Yarlung Gorge is also spatially coincident with Namche Barwa massif in the eastern Himalayan syntaxis and coincides with the highest Pliocene exhumation rates observed on Earth (e.g., Finnegan et al., 2008; Zeitler et al., 2014; Figure 1). Such high exhumation rates at this knickpoint have been interpreted as the consequence of Brahmaputra capture (e.g., Cina et al., 2009; Zeitler et al., 2001), or the coupling of tectonic and surface process through rivers and glaciers (Finnegan et al., 2008; Zeitler et al., 2014). If the former model is correct, it predicts that these knickpoints may potentially migrate upstream from the Yarlung Gorge into the Tibetan Plateau. However, the Yarlung Gorge knickpoint has not propagated as anticipated by a simple fluvial incision model, but instead it appears to have been pinned in the Namche Barwa massif since the Pliocene (e.g., Finnegan et al., 2008). This stagnant knickpoint may form due to local tectonics, probably through crustal folding (e.g., Burg et al., 1998), rather than crustal extension (e.g., Finnegan et al., 2008). In order to understand the development of the Yarlung Gorge through the Pliocene, it is necessary to accurately determine the exhumation histories of other knickpoints in the Yarlung River upstream of the gorge. Interestingly, the other knickzones overlap with north-south trending normal faults in space. What is the role of the extensional faults in controlling the formation of these knickpoints?

Changes in topography driven by valley incision are expected to result in a change in near-surface crustal temperatures, which can be measured using low-temperature thermochronometry (e.g., Shuster et al., 2011). We collected samples from the middle reach of the Yarlung River and its tributaries and conducted apatite (U-Th)/He (AHe), apatite $^{4}He/^{3}He$ and apatite fission track (AFT) analysis. We constructed both forward and inverse thermal-kinematic models constrained by these data to determine permissible exhumation histories along the Yarlung River. The data reveal two stages of rapid cooling since the mid-Miocene. Coupled with regional geological settings, our results confirm that rapid exhumation during the mid-Miocene was regional and coincident with an intensified Asian monsoon and east-west extension. Accelerated exhumation during the Pliocene-Pleistocene was limited to steep, narrow reaches of the Yarlung River coincident and coeval with local tectonic structures.

2 Geological setting

Geologically, the Himalaya is defined by the Yarlung-Zangbo Suture Zone (YZSZ) in the north and the Main Frontal Thrust (MFT) in the south (Yin, 2006), while the Tibetan Plateau is composed of several terranes which were accreted into Asia since the Paleozoic and is bounded by the YZSZ to the south and the Ayimaqin–Kunlun suture zone (AKSZ) to the north (e.g., Wang et al., 2014a). Geographically, southern Tibet usually refers to the Lhasa terrane, the YZSZ and part of the Tethyan Himalaya. Oxygen isotopic compositions from paleosols and lacustrine calcareous carbonates in the Linzhou Basin indicate that the Linzhou area had attained near-present elevation as early as Paleocene-Eocene (60-48 Ma; Ding et al., 2014; Ingalls et al. 2018). In contrast, other stable-isotope paleoaltimetry studies of the Himalayan Neogene basins suggest that they had obtained an elevation similar to modern at around 11-9 Ma (Garzione et al., 2000; Huntington et al., 2015; Rowley et al., 2001). The above geographic evolution of the Lhasa and Himalayas might facilitate the formation of the Yarlung River which straddles both geological units. The Yarlung River generally flows eastward along the YZSZ and then flows southward through the eastern Himalayan syntaxis. The middle reach of the Yarlung River is

characterized by alternating steep gorges and braided valleys (Zhang, 1998; Figure 2a). Four major knickzones have been identified upstream in its middle-western reach (Zhang et al., 2016), which are located at or near the intersection of the Yarlung River and major active north-south-trending fault zones (Figures 2b). These knickzones spatially coincide with steep, narrow gorges. We investigate two key gorges in the middle reach, termed here the Dazhuka-Yueju gorge in the west and the Zedong-Jiacha gorge in the east (Figure 2a).

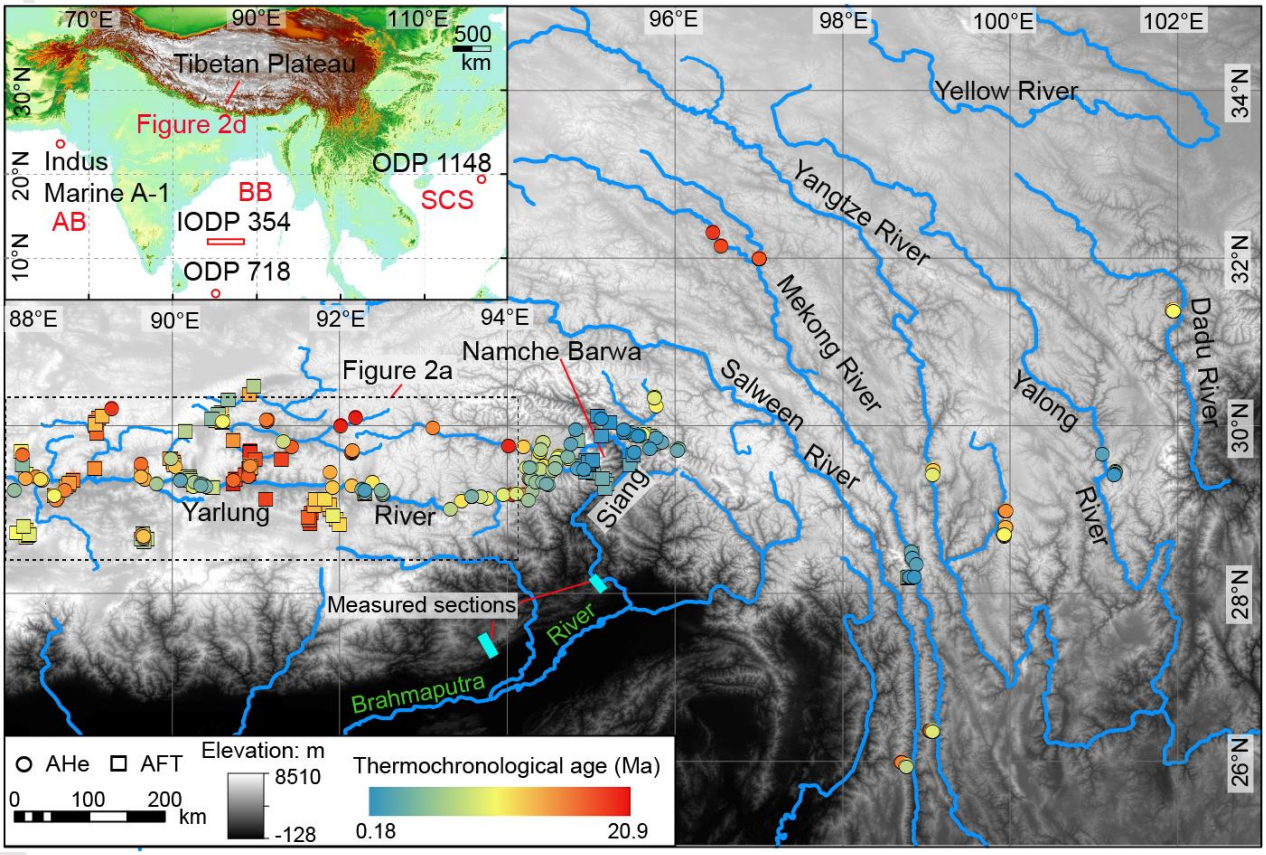

Figure 1. Major drainage settings in the southern and eastern Tibetan Plateau. Topographic map of southern and eastern Tibetan Plateau, showing AHe and AFT ages (Carrapa et al., 2014, 2017; Dai et al., 2013; Ge et al., 2017, 2018, 2020; Gourbet et al., 2019; Ingalls et al., 2018; Lee et al., 2000, 2007; Li et al., 2015, 2016, 2017; Nie et al., 2018; Orme, 2019; Ouimet et al., 2010; Replumaz et al., 2020; Rohrmann et al., 2012; Schmidt et al., 2015; Seward and Burg, 2008; Tremblay et al., 2015; Tu et al., 2015; Wang et al., 2007; Yang et al., 2018; Yu et al., 2011; Yuan et al., 2002, 2009; Zeitler et al., 2014). Locations of measured sections of Siwalik Group are from Lang and Huntington (2014). Inset displays broader geographic context with locations of ODP 1148, well Indus Marine A-1 and IODP (Integrated Ocean Drilling Program) Expedition 354 drill sites those are discussed for environmental indicator, total sediment flux (Clift et al., 2008) and detrital zircon age (Blum et al., 2018). The red line represents the location of a schematic cross-section of southern Tibet in Figure 2d. SCS, South China Sea; AB, Arabian Sea; BB, Bengal Bay.

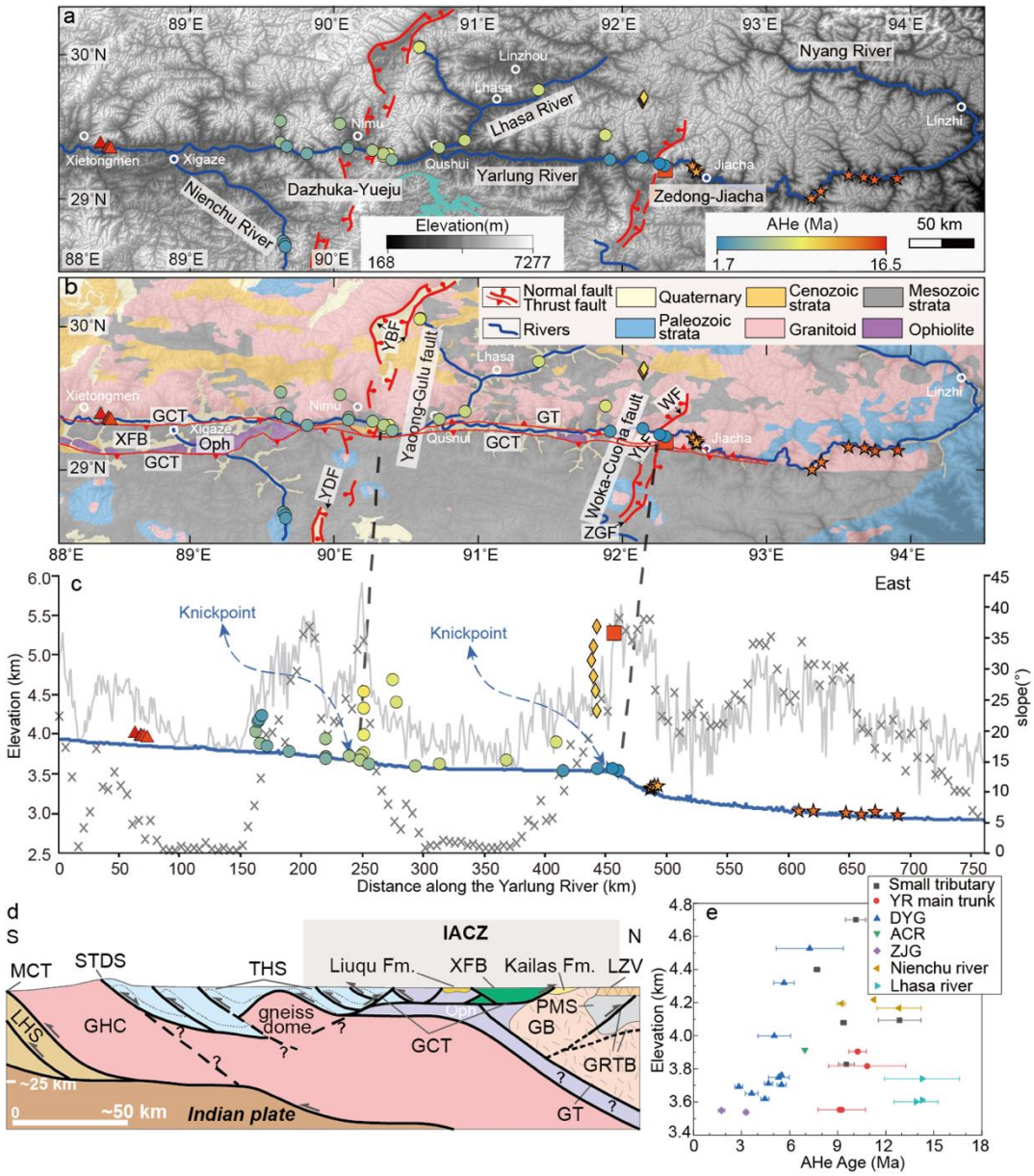

Figure 2. (a) Middle reach of the Yarlung River and its tributaries showing sample locations and AHe ages. Circle, this study; triangle, Dai et al. 2013; star, Schmidt et al. 2015; diamond, Tremblay et al. 2015; square, Li et al. 2015; these points representing AHe ages are the same in a, b and c. The Dazhuka-Yueju and Zedong-Jiacha are two gorges. (b) Simplified geological map (modified from Pan et al. 2004) of the southern Tibet showing the major different lithologies, and two north-south rifts. (c) Yarlung River profile showing local slope (crosses). The grey line is the maximum elevation within the buffer area, while the blue line is the minimum elevation. (d) Schematic cross-section across the Gangdese arc, the Yarlung Zangbo Suture Zone, the Tethyan Himalaya (modified from Orme et al. 2015). (e) Mean AHe age versus sample elevation. YBF, Yangbajin fault; YDF, Yadong fault; WF, Woka fault; YLF, Yalaxiangbo fault; ZGF, Zhegu fault; GT, Gangdese thrust; GCT, Great Counter thrust; STDS, South Tibetan Detachment System; MCT, Main Central Thrust; GRTB, Gangdese Retroarc Thrust Belt; XFB, Xigaze Forearc basin; Oph, Ophiolite; GB, Gangdese Batholith; PMS: Paleozoic-Mesozoic Strata; LZV, Linzizong Volcanics; LHS, Lesser Himalayan Sequence; GHC, Greater Himalayan Sequence; THS, Tethyan Himalayan Sequence; Fm., Formation; IACZ, Indian-Asian Collision Zone; YR, Yarlung River; DYG, Dazhuka-Yueju Gorge; ZJG, Zedong-Jiacha Gorge; ACR, Adjacent Canyon Rim.

In general, the Dazhuka-Yueju gorge is located in the center of the north-south (N-S) trending Yadong-Gulu fault (Harrison et al., 1992), while the Zedong-Jiacha gorge is located in the N-S trending Woka-Cuona fault zone (Zhang et al., 2016; Figure 2b). In the Dazhuka-Yueju gorge, the Yangbajin (YBF) and Yadong (YF) normal fault developed to the north and south of the Yarlung River, respectively. In the Zedong-Jiacha gorge, the west-dipping Woka (WF) fault developed north of the Yarlung River, while the west-dipping Zhegu (ZGF) fault, the east-dipping Yalaxiangbo (YLF) and Cuona fault (CNF) developed south of the river (Zhang et al., 2016; Figure 2b). For the southern Tibetan Plateau and Himalayas, estimates for the initiation of the N-S trending normal faults range from 20 Ma to 2 Ma (e.g., Bian et al., 2020; Sundell et al. 2013; Styron et al. 2013; Langille et al. 2012; Laskowski et al. 2017), but the majority of extensional faulting began in the mid-Miocene (15-10 Ma; as summarized in Sundell et al., 2013 and Wolff et al., 2019). Between these two steep gorges, the Yarlung River is wide and braided with shallower slopes (Figure 2c). The Yarlung River and its tributaries cut through both the Tethyan Himalayan rocks to the south, and the Gangdese granitoid batholiths to the north (Figure 2b). These batholiths provide suitable minerals for thermochronometry and an ideal chance to extract exhumation histories (Cao et al., 2020) along the Yarlung River.

The middle reach of the Yarlung River occurs within the Indian-Asian Collision Zone (IACZ; Figure 2). In the western part of our study area, the IACZ consists of the Gangdese arc (e.g., Zhu et al., 2011), the Kailas Formation (deposition at 26-21 Ma, Decelles et al., 2011), the Xigaze forearc basin (e.g., Orme and Laskowski, 2016), the Yarlung Zangbo ophiolite (e.g., Dai et al., 2020) and the Tethyan Himalaya (e.g., Kapp and DeCelles, 2019; Yin, 2006; Figures 2b and 2d); while in the eastern part, the north-dipping Gangdese thrust (GT) juxtaposes the Gangdese arc over Tethyan Himalayan sequence (THS), and the south-dipping Greater Counter thrust (GCT) juxtaposes the THS over the Gangdese granitic rocks, both of them resulting in the disappearance of the Xigaze forearc basin (Yin et al., 1994; Figures 2b). The timing of the GT movement was estimated to be 27-23 Ma by $^{40}Ar/^{39}Ar$ thermochronology data (Yin et al., 1994), whereas that of the GCT was constrained to be 23-16 Ma by the field relationship that the GCT cuts the Kailas Formation, and the GCT was crosscut by local faults (movement as early as 16 Ma; Laskowski et al., 2018).

3. Analytical methods

Samples were crushed and apatite crystals were separated using standard heavy liquid and magnetic separation techniques. For apatite (U-Th)/He measurements, individual apatite crystals were selected and photographed under a polarizing stereographic microscope. Euhedral, inclusion-free, unfractured crystals were selected and measured for geometric parameters to calculate α-ejection corrections (Farley, 2002). The measured grains were packaged into Nb tubes, loaded into an ultra-high vacuum laser microfurnace, and heated with a 70 W, 810 nm-wavelength diode laser to ~1050 ºC. The extracted gas was spiked with pure ^{3}He, exposed to getter pumps to remove reactive gases, and cryogenically separated to isolate helium. Helium content was then measured by isotope dilution on a Pfeiffer Prisma quadrupole mass spectrometer QMS 200 under static vacuum in the Noble Gas Thermochronometry Lab at Berkeley Geochronology Center (BGC). Following He extraction and analysis, apatite grains were dissolved and the abundances of U, Th, and Sm were measured by isotope dilution using a Thermo Scientific Neptune Plus multi collector inductively coupled plasma mass spectrometer (ICP-MS) at the BGC. Most samples have AHe analyses on three apatite grains. AHe analytical data are provided in Table S1.

Measurements for apatite $^4He/^3He$ thermochronometry were also made in the Noble Gas Thermochronometry Laboratory at BGC. To generate ^3He, several hundred apatite grains from each sample were irradiated with protons at the Francis H. Burr Proton Therapy Center at the Massachusetts General Hospital in Boston, Massachusetts, USA, in November 2014 with protons of ~220 MeV incident energy for 6 Hours. The total proton fluence for this irradiation was 1×10^{16} protons/cm^2. Following irradiation, individual apatite crystals were selected and their geometric parameters were measured, as described above for AHe analyses. Selected grains were placed inside platinum packets and heated in a sequence of increasing temperature steps in the ultra-high vacuum laser microfurnace. The extracted gas in each step was purified as described above, and the helium isotopic composition was measured using an MAP 215-50 sector field mass spectrometer in pulse counting mode. Following step heating measurements, abundances of U, Th, and Sm were measured by solution ICP-MS following the same procedure as for AHe analyses. A highly detailed description of these AHe and $^4He/^3He$ analytical procedures are reported in Tremblay et al. (2015). Apatite $^4He/^3He$ analytical data are provided in Table S2.

Fission track ages, track lengths, and Dpar measurements were performed at the State Key Laboratory of Earthquake Dynamics, Institute of Geology, China Earthquake Administration, using the external detector method (Donelick et al., 2005) and the zeta calibration technique (Huford and Green, 1983). Samples were irradiated at the USGS TRIGA Reactor in Oregon, USA. Apatite grains were irradiated together with IRMM 540R dosimeter glass to check the constancy of the neutron flux. The AFT data were reported in Table S3. The central age was calculated using TrackKey (Dunkl, 2002) and its uncertainty or age error was calculated according to Galbraith and Laslett (1993).

4 New thermochronometric data

We report 82 single-grain AHe ages from 28 samples from both the Dazhuka-Yueju and Zedong-Jiacha gorges and braided valleys of the main Yarlung River trunk and its tributaries (Figure 2b and Table S1). The overwhelming majority of samples were collected from river-level plutonic rocks (Figures 2a and 2b). Four samples were analyzed for $^4He/^3He$ (Table S2), and one sample was analyzed for AFT (Table S3). The published AHe age data from the river valleys have been compiled (Figure 2a).

The single-grain AHe ages of most samples from the Yarlung River are consistent, however, some samples show some dispersion with anomalously old ages (Table S1). These anomalously old ages are ages that are 50% older than the mean of other replicates, and they are excluded in the following discussion. AHe ages display neither any positive correlation with eU (effective Uranium) concentration nor with crystal radius (Figure S1), and they can basically be separated into two groups. AHe ages from the braided valleys of the Yarlung River and its tributaries are mainly concentrated in the mid-Miocene, whereas those from the gorges are scattered throughout the Pliocene-Pleistocene (Figure 2a).

AHe ages from the braided valley of the Yarlung River and its small tributaries range from 9.1 Ma to 12.8 Ma. In the two main tributaries of the Yarlung River, the Lhasa and Nienchu Rivers ages range from 13.9 Ma to 14.3 Ma and from 9.3 Ma to 12.8 Ma, respectively (Figures 2a, 2e and S1). Two samples from an elevation profile of 300 m in the Lhasa River tributary yield an average age of 10.1 Ma (4,700 m) and 7.2 Ma (4,400 m), which are much younger than other AHe ages in its main trunk and are possibly related to the Yangbajin fault activity (Figure 2a).

AHe ages of river-level samples from the Dazhuka-Yueju gorge range from 2.8 Ma to 5.5 Ma, whereas samples from the Zedong-Jiacha gorge are as young as 1.8 Ma and 3.3 Ma, younger than previously published AHe ages further to the east that are concentrated between 4.8 Ma and 5.8 Ma (Schmidt et al., 2015; Figures 2b and 2e). In the Dazhuka-Yueju gorge, four samples from top to bottom of one 780-m elevation transect have AHe ages of 7.3 Ma, 5.7 Ma, 5.0 Ma, 5.3 Ma, and one AHe age of one sample from the adjacent gorge rim is ca. 7 Ma. One reported AFT age of the Dazhuka-Yueju gorge is ca. 6.9 Ma (Copeland et al., 1995), while one AFT age from the youngest AHe sample in the Zedong-Jiacha gorge is ca. 9 Ma (Figure 2b). In order to extract more thermal information, thermal history and thermokinematic numerical modelling was conducted.

5 Thermal history and thermokinematic numerical modelling

5.1 Thermal history from QTQt modelling

The thermal histories have been modelled using the software QTQt, which is based on a trans-dimensional Bayesian Markov Chain Monte Carlo method (Gallagher, 2012). We conducted inverse simulations assuming He diffusion kinetics in apatite as prescribed by the radiation damage model of Flowers et al. (2009). Given that the range of temperature sensitivities for the thermochronometers (AFT and AHe) we have data for, we imposed explicit constraints of 160±30 °C during the time 25±15 Ma and of 70±70 °C from now to twice the oldest age in the thermal history models (Gallagher, 2012). We also impose a no reheating restriction in the QTQt models.

On the basis of similar AHe ages and topographic characteristics, at least two river-level samples have been modelled together in a particular location. For the Zedong-Jiacha gorge, sample DJG14-03 and DJG14-02 have been jointly modelled, whereas for the Dazhuka-Yueju gorge, samples DJG14-66, DJG14-68, L06-04, L07-01 and L07-02 have been modelled together. For the braided valley in between the two gorges, samples DJG14-05, DJG14-08, DJG14-63 have been used. For the braided tributaries of the Yarlung River, we used samples L07-12 and L08-05 for Lhasa river, samples DJG14-61 and DJG14-62 for Nienchu river, and sample L03-12 and L05-13 for the small tributary. All the modelling results are shown in Figures 3 and S2.

5.2 Thermal history from apatite $^{4}He/^{3}He$ data

To determine which thermal histories are consistent with the apatite $^{4}He/^{3}He$ data, we employed the algorithm presented in Schildgen et al. (2010). Using this algorithm, we tested 2000 random cooling paths with initial temperatures of 150 ºC and starting times at least four times greater than the AHe age of a particular sample (i.e., 10 Ma for DJG14-66 and DJG14-03; 40 Ma for DJG14-08 and L05-13). Model thermal paths end at the present-day and at a temperature of 0 °C, within the range of modern mean annual temperature (MAT) expected for our sample elevations in southern Tibet (0.1 to –9.0 °C; Quade et al., 2011). If a cooling path did not predict the observed (U-Th)/He age within analytical uncertainty, it was colored grey; if it did predict the observed age, it was colored red, yellow or green based on the misfit between the predicted and observed $^{4}He/^{3}He$ spectrum using a statistic M described by Schildgen et al. (2010) (red, $M \geq 4$; yellow, $M < 4$; green, $M < 2$). Cooling paths constrained from apatite $^{4}He/^{3}He$ data of each sample are shown in Figure 4.

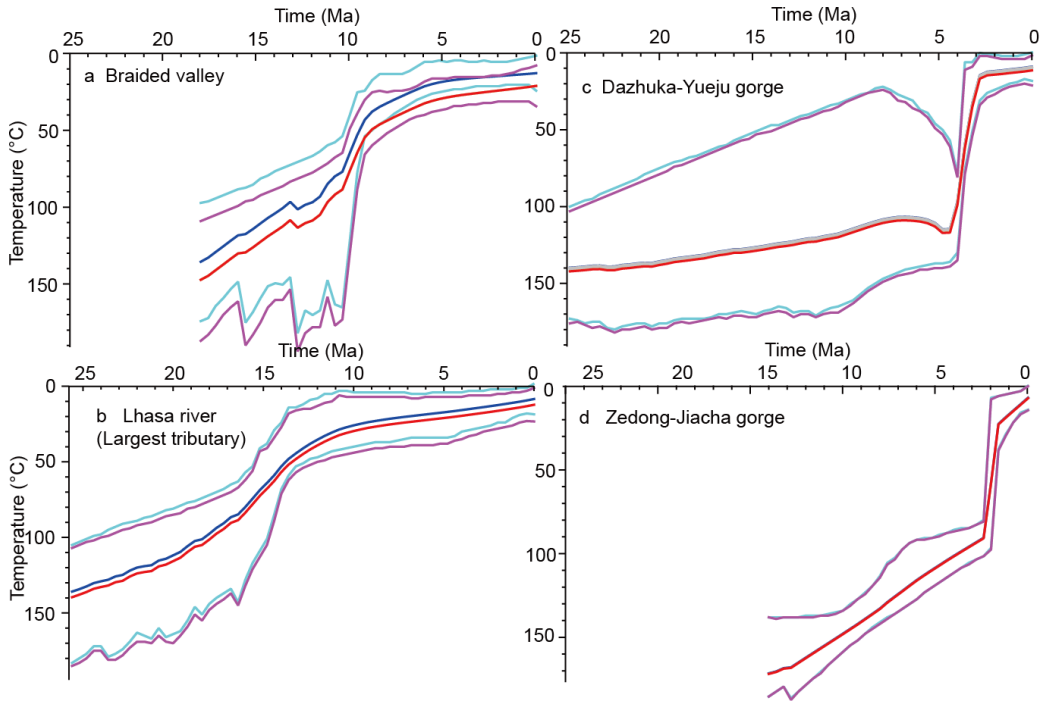

Figure 3. Expected thermal histories of samples in the middle reach Yarlung River using QTQt. Extracted thermal histories of the braided valley (a), the Lhasa river (b), the Dazhuka-Yueju gorge (c) and the Zedong-Jiacha gorge (d) inferred from AHe and AFT data employing the radiation damage model of Flowers et al. (2009). In panels a-d, blue lines represent thermal history of the uppermost sample, whereas the cyan lines are 95% credible intervals; red lines represent thermal history of the lowermost sample, while the magenta lines are 95% credible intervals. The grey lines represent thermal histories for all samples in between them (see Figure S2 for details).

5.3 Thermokinematic numerical modelling from Pecube

We performed thermokinematic modelling using the Pecube code (Braun et al., 2012). Pecube solves the heat production, conduction, and diffusion equation for a given 3D kinematic field, and thus allows to explore the effects of tectonic heat transport and erosion on the thermal structure of the crust, mineral cooling ages and histories. We use Pecube forward models to predict thermochronological ages at the present-day surface (Table S4). We also use inverse models to explore the sensitivity of the model to changes in a specific model parameter (Table S5). Inverse modelling can constrain input parameters such as fault slip rate and relief history through comparing observed data and predicted ones (Braun et al., 2012). Here we explore one model parameter at a time so that the input parameter is free while other parameters are held constant at reference values, following Carrapa et al. (2016).

The ASTER 30 m global digital elevation model (GDEM) has been used for the present-day surface. We conducted different models for the Zedong-Jiacha gorge (Figures 5, S3a and S3b) and the Dazhuka-Yueju gorge (Figure S3c), respectively. Both models simulate 10 Ma of exhumation. For each set of models we impose the same thermal parameters that lead to a modern average geothermal thermal gradient of approximately 30 ℃/km (Jiang et al., 2019) with a thermal diffusivity of 25 km^2/Ma; a temperature at the base of the model of 915 ℃, a temperature at the sea level of 15 ℃, an atmospheric lapse rate of 6 ℃/km and a heat production of 0 ℃/Ma (Braun et al., 2012; Table S4). It is important to note that the exact geothermal gradient evolves through time due to exhumation and varies spatially due to fault slip and

topography. We explore the sensitivity of our results to the temperature at the base of the model in Table S5.

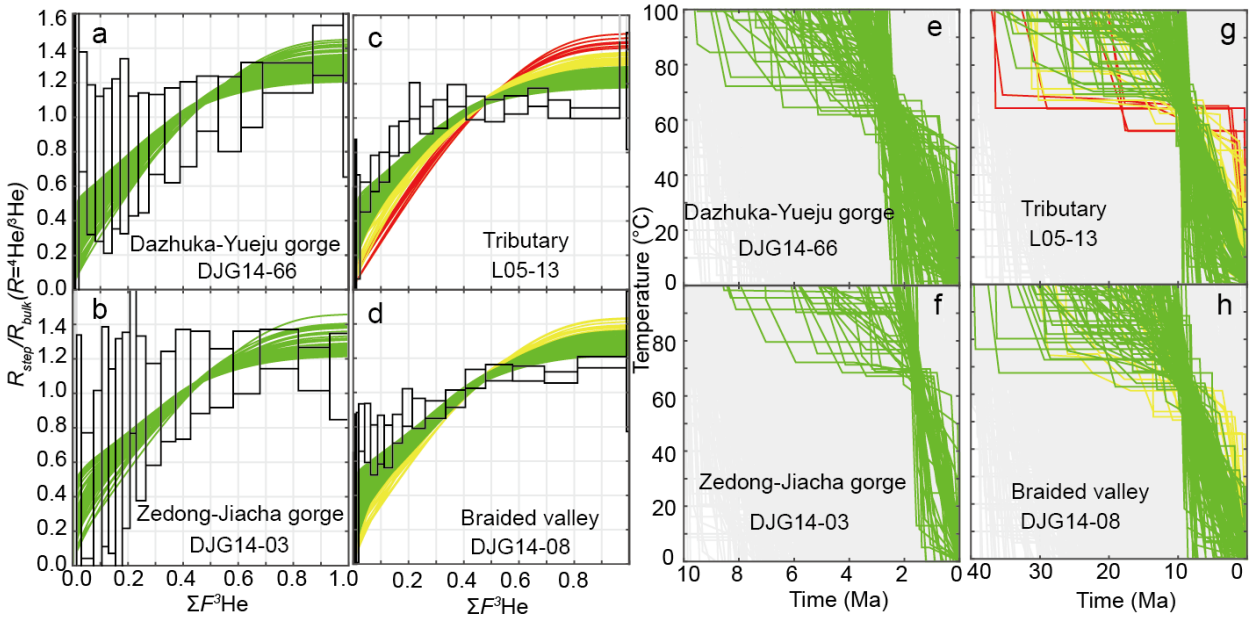

Figure 4. Apatite ^{4}He/^{3}He thermochronometry of samples from braided valley (DJG14-08), small tributary (L05-13), the Dazhuka-Yueju gorge (DJG14-66) and the Zedong-Jiacha gorge (DJG14-03). Normalized ^{4}He/^{3}He ratios (R_{step}/R_{bulk}) are plotted as a function of cumulative ^{3}He released (ΣF^3He) during stepwise degassing analysis of each sample (a-d). Modeled cooling paths (2,000 times randomly) and their level of agreement with the observed ^{4}He/^{3}He data (e-h). Colored cooling paths predict the observed (U-Th)/He age within analytical uncertainty (1σ), whereas the gray paths do not. Green cooling paths are most consistent with the observed ^{4}He/^{3}He release spectra, yellow and red cooling paths are progressively less consistent. For the gorge samples, the ^{4}He/^{3}He datasets are characterized by large uncertainties in the observed ^{4}He/^{3}He, which prevent us from constraining these samples' thermal histories beyond what is constraint by the conventional (U-Th)/He age. For the tributary and braided valley samples, the ^{4}He/^{3}He data indicate that rapid cooling within the last ~5 Ma is not likely.

For the Zedong-Jiacha gorge, we explore two different scenarios with and without a normal fault to evaluate its impact. This normal fault is west-dipping, two samples from the eastern parts are located in the footwall and three samples from the western part are distributed in the hanging wall. The hanging wall moves westward with respect to the footwall (Figures 2a and 5a). We compared the model-predicted age patterns with the observed data (Figure S3b). In the model with a normal fault, the model is subdivided into three stages (See discussion section): the fault was not active during stage 1 (10-4 Ma) and stage 3 (1.5-0 Ma), while the fault was active at various rates (0-5 mm/a) during stage 2 (4-1.5 Ma). These durations are based on the results of the QTQt models but we test this duration below. In the model without a normal fault, the uplift rate is uniform across the model domain. The lowest misfit values for these two models were obtained by inverse modelling with respect to a reference model. The lowest misfit of the model without a normal fault is ~270, which is 15 times greater than the misfit for a model with the normal fault. This model predicts older ages for two samples in the footwall than we observe (Figure S3b). In contrast, the model with a normal fault predicts cooling age patterns similar to observations, with a lowest misfit of ~18 (Figure S3b).

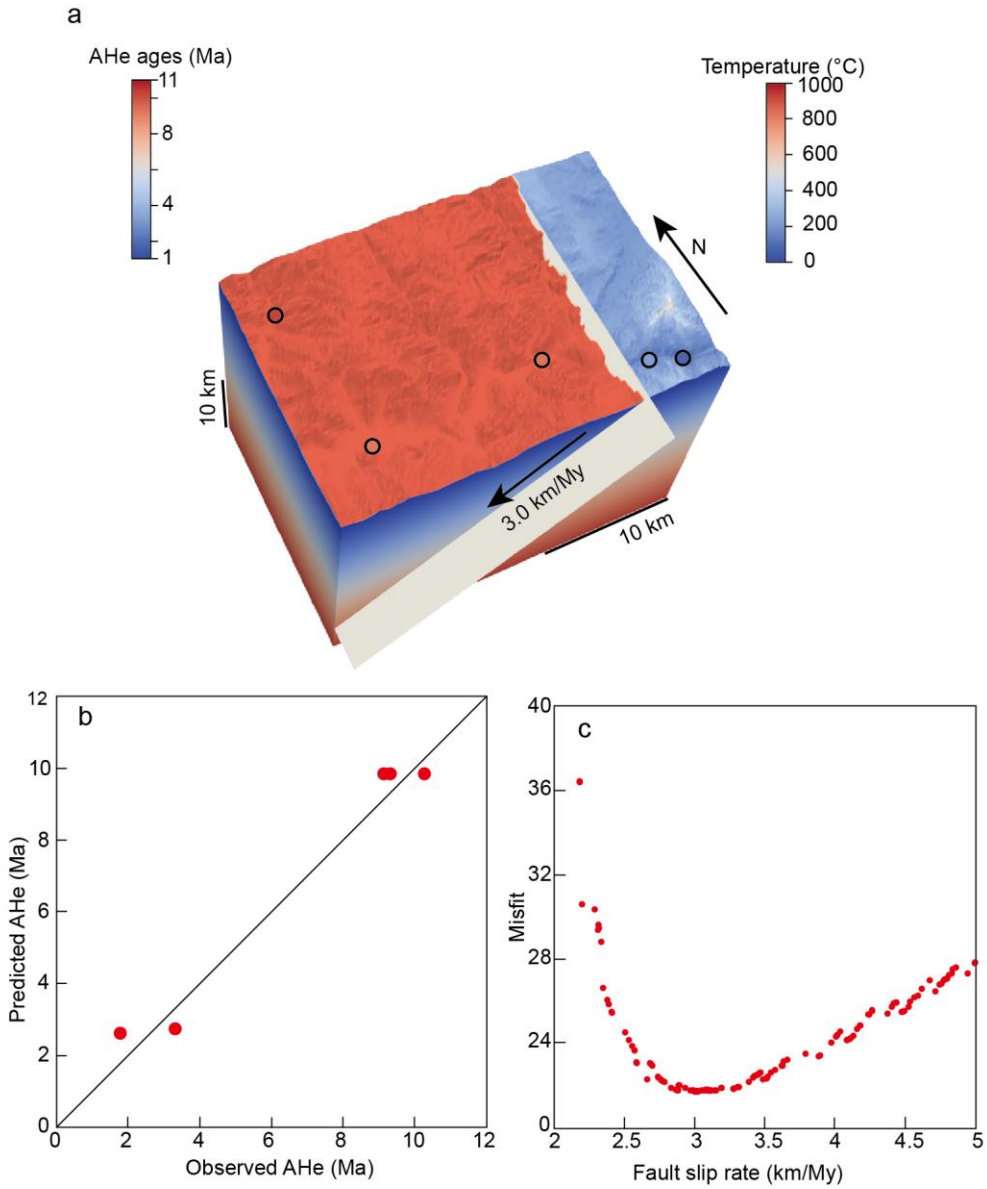

Figure 5. Forward and inverse 3D thermokinematic model using Pecube (Braun et al., 2012). (a, b) Predicted forward modelling ages for a scenario in which western dipping fault was localized in the Zedong-Jiacha gorge. Circles represent AHe ages (Ma). (c) Fault slip rates inferred from inverse model based on the misfit (the lower the misfit, the better the model; see the modelling section and Figure S3 for details).

For the Dazhuka-Yueju gorge, due to the complexity of the normal fault distribution, only one scenario has been explored that includes the geometry of a fault. Three stages of fault motion have been defined on the basis of previous studies (See discussion section): the fault was not active during stage 1 (10-8 Ma) and stage 3 (3-0 Ma), while the fault was active at various rates (0-5 mm/a) during stage 2 (8-3 Ma). The forward models with faults for both gorges (Figures S3a and S3c) predicted AHe ages which are consistent with observed ages.

The one-dimensional inversions for fault slip rate, fault angle, basal temperature, and end of the fault activity for the Dazhuka-Yueju and Zedong-Jiacha gorges are presented in Figures 5, S3a, S3c and Table S5, respectively.

6 Discussion

6.1 Mid-Miocene exhumation of the Yarlung River braided valley and tributary

AHe ages from the braided valley and tributary are mainly concentrated around the mid-Miocene (Figure 2b). AFT ages from the braided sections of the Yarlung River and Lhasa River cluster around 15-20 Ma (Figures 1 and 6b), and the early Miocene exhumation was related to activity of Gangdese thrust (Copeland et al., 1995; Dai et al., 2013). There is overlap between AFT and AHe ages (Figure 6b), suggesting rapid exhumation at approximately 15 Ma. This inference is supported by thermal modelling that reveals river-level samples from the Lhasa River underwent rapid cooling from ca. 80 °C to ca. 20 °C during 15-10 Ma (Figures 3b and S2d). The stage of rapid cooling was accelerated during 11-9 Ma with cooling from ca. 100 °C to ca. 30 °C according to the thermal modelling results from samples in the braided valleys, small tributaries and the Nienchu River (Figures 3a, S2c, S2e, S2f). The cooling history of one sample from the braided valley (Figures 4d and 4h) and another sample from the small tributary (Figures 4c and 4g) derived from apatite $^{4}He/^{3}He$ and AHe data also reveal a period of rapid cooling around 10-9 Ma. Considering that the lack of coeval magmatic activity in the sampled area during cooling stages (Cao et al., 2020; Zhu et al., 2011), we tend to think that the cooling is mainly caused by exhumation. Assuming a geothermal gradient of ~25-30 °C/km, the river-level samples from the braided sections of the Yarlung River and tributaries were exhumed from 2.8-2.0 km depth to near-surface temperatures during 15-9 Ma, and have experienced remarkedly slow erosion rates since then.

The mid-Miocene stage of rapid exhumation reported here is compatible with the exhumation history in the IACZ recorded by thermochronometric data from both plutonic and sedimentary rocks (Dai et al., 2013; Li et al., 2016; Figure 1). Apatite $^{4}He/^{3}He$, AHe, and ZHe ages and thermokinematic models from an elevation transect from granitoids in the central Gangdese (Figure 2a) also indicate a stage of rapid exhumation of 1 km/Ma during 17-11 Ma (Tremblay et al., 2015). Detrital AFT ages from the Kailas Formation (26-21 Ma; Leary et al., 2016) in the IACZ range from ca. 14 to 18 Ma have been interpreted to be fully reset by burial, and therefore indicate significant erosional unroofing (Carrapa et al., 2014). Similarly, AFT ages of the Upper Triassic sandstones in the northern Tethyan Himalaya mainly cluster at ca. 12-8 Ma (Li et al., 2015). In addition, there is an increase in the proportion of the Gangdese detrital zircons during the mid-Miocene in the Indo-Burma Range (IBR) (Betka et al., 2019).

The above observations suggest that the mid-Miocene rapid exhumation occurred simultaneously across the IACZ in the southern Tibetan Plateau (Figure 6b). Given that timing of Gangdese thrust (27-23 Ma, Yin et al., 1994) and Greater Counter thrust activity (23-16 Ma, Laskowski et al., 2018; Figure 6d), this stage of exhumation is likely related to high erosion rates along the Yarlung River (Carrapa et al., 2014; Li et al., 2015). However, the onset timing of the N-S trending normal faults in southern Tibetan Plateau and the Himalayas was mainly in the mid Miocene (15-10 Ma; e.g., Sundell et al. 2013; Styron et al. 2013; Figure 6d). This stage of extensional faulting led to extensive exhumation of the footwalls of normal faults, which suggests that the extensional tectonics is a possible major contributor to the regional rapid mid-Miocene exhumation rate in the IACZ. In addition, it has been proposed that the India plate was thrust under southern Tibet during the Early Miocene, following slab-breakoff of Greater India (DeCelles et al., 2011). This would drive rapid rates of rock uplift and exhumation (DeCelles et al., 2011; Carrapa et al., 2014).

Is it possible that this stage of rapid exhumation was related to the drainage reorganization? Tremblay et al. (2015) proposed a transition from transverse drainage across paleo-Himalayas to longitudinal drainage in the IACZ to explain the dramatic decrease in erosion rates since 11-10 Ma across the Southern Tibetan Plateau. If so, this model predicts that the IACZ was drained by south-flowing drainage systems and moisture was steered northwards into the IACZ along these drainages pre-10 Ma. This is supported by the observation that the Himalayas did not obtain their current high elevations until 11-9 Ma as evidenced by the stable isotopic paleoaltimeters (Garzione et al., 2000; Huntington et al., 2015; Rowley et al., 2001; Figure 6d). Thus, the mid-Miocene high exhumation rates are hypothesized to result from a combination of steeper rivers and higher precipitation rates. This south-flowing drainage model is possible under the condition that the modern east-flowing Yarlung River (i.e., the Yarlung-Brahmaputra drainage) was not established pre-10 Ma.

The timing for the establishment of the modern Yarlung-Brahmaputra drainage via the Siang River ranges from ca. 18 Ma (Robinson et al., 2014), Early Miocene (Bracciali et al., 2015), ca. 7 Ma (Chirouze et al., 2013), to ca. 3-4 Ma (Cina et al., 2009). More recent studies based on the provenance analysis of both the proximal deposits of the Lower Siwalik Group (cf. Lang and Huntington, 2014; Lang et al., 2016; Figure 1) and the distal deposits of IODP core (cf. Blum et al., 2018; Figure 1 insert) reveal that the occurrence of Gangdese zircons as early as >13 Ma and >18 Ma, respectively. The proportion of Gangdese arc increases up section from ~3% within the Oligocene to early Miocene strata to ~30% within the late Miocene-Pliocene strata in the Indo-Burma Range (IBR) suggesting that the cross-suture drainage might be established by at least the Oligocene-Miocene boundary (Zhang et al., 2019; Betka et al., 2019). Even though, the above observations cannot rule out the south-flowing drainage systems, such as the Subansiri-Brahmaputra (Cina et al., 2009), the integration of the Yarlung-Siang-Brahmaputra is most likely to have occurred by the early Miocene. Interestingly, Leary et al. (2016) proposed the early Miocene Liuqu Conglomerate represents the southern part of the Yarlung River catchment based on the observation that it has both north and south sources from the Gangdese and the mélange, respectively. This scenario is reasonable because elevations across the Himalayas are expected to increase since at least the early Miocene through duplex fault systems (Grujic et al., 2002, 2020; Long et al., 2011), even if it did not obtain its current elevation. The surface uplift in the Himalayas might have facilitated the formation of longitudinal rivers parallel to the orogenic belt. It should be noted that the depositional age of the Liuqu Conglomerate is not well constrained, and one recent study indicates it was deposited during the Paleocene (Ding et al., 2017).

The mid-Miocene phase of rapid exhumation is not limited in the IACZ, but it is a regional geological event. For example, AHe data of bedrock samples collected at river-level from the upper and lower reaches of the Mekong River in the southeastern Tibetan Plateau revealed a stage of rapid exhumation in the mid-Miocene (Figure 1; Nie et al., 2018). Therefore, other factors including climate may control the mid-Miocene erosion rates. Notably, environmental indicators including mineralogical ratio chlorite/(Chlorite+haematite +goethite) (C_{RAT}) and Chemical Index of Alteration (CIA) from Neogene sediments (Figure 1 inset) of the South China Sea (ODP site 1148) and Arabian Sea (Indus Marine A-1) suggest particularly high precipitation rates from 15 Ma to 10 Ma ago due to Indian and East Asian summer monsoon strength (Clift et al., 2008; Figure 6a). This mid-Miocene intensified monsoon would increase the precipitation rates, increasing river discharge, and thus erosion rates (Nie et al., 2018; Figure 6c). Because it is difficult to accurately reconstruct the paleo-morphological features of southern

and eastern Tibet, it is challenging to evaluate whether the high precipitation rates caused by the intensified monsoon would be uniform across the large geographic area. Here we argue that the coeval exhumation acceleration across the large, externally-drained Tibetan Plateau might be associated with monsoon strength. Additionally, this stage of large-scale exhumation in the IACZ provides enormous volumes of continental material to the Bengal Fan which resulted in the occurrence of Gangdese provenance as early as ca. 18 Ma with a continuous increase during the mid-Miocene (Blum et al., 2018). Similarly, Nie et al. (2018) noticed this stage of rapid erosion in the Mekong River coincides with the enhanced Eastern Asian summer monsoon precipitation during the Middle Miocene Climatic Optimum (MMCO), and they proposed that this rapid erosion was controlled by the high monsoon precipitation rates given that absence of regional tectonic deformation. It is important to stress, however, that climate-driven erosion can only erode topography that is present. As discussed above, a tectonic feedback mechanism is required to sustain high rates of erosion to produce the large amounts of exhumation constrained by the thermochronology, which is estimated to be about 6.4 km in the IACZ (Orme, 2019).

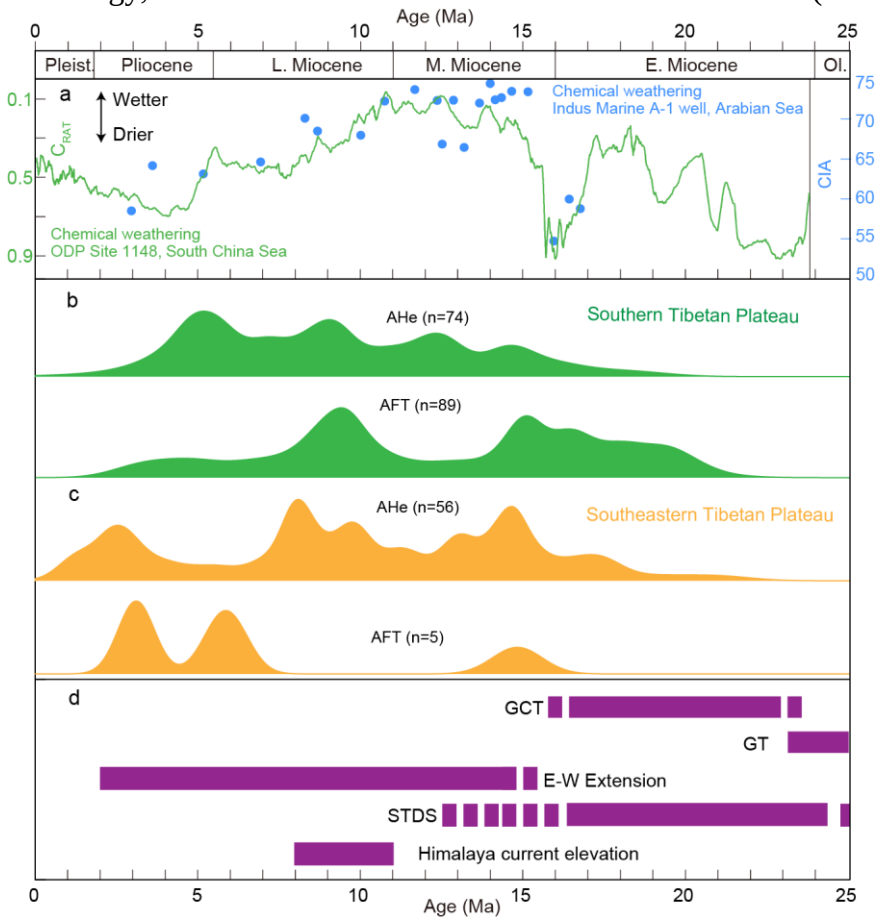

Figure 6. Correlation of climate proxies, low-temperature thermochronological ages and tectonic events. (a) The chemical weathering index CRAT of sediments from ODP Site 1148, South China Sea and CIA data from well Indus Marine A-1, Arabian Sea (Clift et al., 2008). (b, c) Probability distribution functions of compiled thermochronological data of southern and southeastern Tibetan Plateau (the same data source in Figure 1). (d) Tectonic activities in the southern Tibetan Plateau. Timing of South Tibetan Detachment System (STDS, Webb et al., 2017), Gangdese Thrust (GT, Yin et al., 1994), Greater Counter Thrust (GCT, Laskowski et al., 2018), E-W extension (Bian et al., 2020; Sundell et al. 2013; Styron et al. 2013; Langille et al. 2012; Laskowski et al. 2017) and obtaining their current elevations of the Himalayas (Garzione et al., 2000; Huntington et al., 2015; Rowley et al., 2001).

6.2 Pliocene-Pleistocene exhumation of the Yarlung River gorge

Most AHe ages of river-level samples in the gorges are Pliocene-Pleistocene. Thermal histories derived from AHe ages by QTQt inverse modelling (Gallagher, 2012) reveal rapid cooling from ca. 100 °C to ca. 20 °C occurred during ca. 5-3 Ma for the Dazhuka-Yueju gorge (Figures 3c and S2a), whereas accelerated cooling from ca. 70°C to ca. 20°C occurred at ca. 2 Ma in the Zedong-Jiacha gorge after ca. 8 Ma of residence at temperatures of 90-70 °C, inferred from both AHe and AFT ages (Figures 3d and S2b). The above cooling histories are consistent with those from the $^{4}He/^{3}He$ data (Figures 4e and 4f). However, the reported early Pliocene AHe ages (Schmidt et al., 2015) indicate the initiation of cooling for the Zedong-Jiacha gorge might be as early as 5 Ma, similar to that of the Dazhuka-Yueju gorge.

This acceleration in exhumation rate of the above two gorges is coeval with that of the Yarlung Gorge which was constrained from both bedrock and detrital thermochronological data (Finnegan et al., 2008; Gemignani et al., 2018; Govin et al., 2020), as well as worldwide rapid exhumation rates. A worldwide compilation of bedrock thermochronometric ages appears to reveal that mountain exhumation rates, regardless of latitudes, have increased since 6 Ma and most rapidly since 2 Ma (Herman et al., 2013). The worldwide increased mountain exhumation rate temporally corresponds to the increased sedimentation rate and grain size in both active and inactive mountain ranges (Zhang et al., 2001), as well as the global climate cooling recorded by benthic foraminifera oxygen isotope (Zachos et al., 2001). It suggests that late Pliocene-Quaternary climate fluctuation (e.g., Zachos et al., 2001) could be a major control for this stage of worldwide rapid mountain exhumation (Herman et al., 2013). However, an analysis of 30 mountainous locations with accelerated late Cenozoic exhumation recorded by low-temperature thermochronological ages suggested that many of these locations were controlled by tectonic activity (Schildgen et al., 2018). Thus, alternatively, local and regional tectonic activity might control exhumation rate (Schildgen et al., 2018). It remains debated whether this global signal is related to tectonics or climate (Fox and Carter, 2020; Willett et al., 2020).

Here, we propose that this acceleration is associated with local tectonics due to the spatial coincidence of the gorges with the N-S trending rifts in the southern Tibetan Plateau. Our new thermochronometric data paired with existing thermochronometry (Bian et al., 2020) support the idea that the young AHe ages result from motion on the N-S trending normal faults. Relevant for the Dazhuka-Yueju gorge, ^{40}Ar-^{39}Ar ages of biotite and K-feldspar, and AFT ages from gneissic granitic rocks in the Yangbajin shear zone reveal the timing of significant motion on the Yadong-Gulu normal fault should be between 8 and 3 Ma (Harrison et al., 1992; Pan and Kidd, 1992). For the Zedong-Jiacha gorge, AFT and AHe data indicate the Woka and Cuona footwalls have been rapidly exhumed since ca. 3.8 Ma (Li et al., 2015) and ca. 3-2.3 Ma (Bian et al., 2020), respectively. Obviously, timings of normal fault tectonic denudation within the two rifts are coeval with those of exhumation within the gorge portion of Yarlung River. Such good coincidence in space and time between rift zones and river gorges, integrated with the regional slow exhumation rates in the IACZ since 10 Ma (Tremblay et al., 2015), indicates that exhumation of the gorge is controlled by local normal fault activity. Normal faults cut across the river and formed a series of local steepened river reaches, which increase erosion rates of these areas (Zhang, 1998). It is also important to note that the river evolution is a function of signals that migrate upstream. The tectonic processes shaping the Yarlung Gorge, downstream of our study area, are expected to exert a control on transient incision. Schmidt et al. (2015) showed that the fluvial knickpoint associated with the Zedong-Jiacha gorge can also be identified in tributaries. Celerity modelling support the idea that the knickpoint in the Zedong-Jiacha gorge

and tributaries are genetically linked to tectonic activity just above the Yarlung Gorge. Furthermore, Wang et al. (2014b) reveal large thicknesses of sediments immediately above the Yarlung Gorge, suggesting that enhanced rock uplift of Nambche Barwa ~2 million years ago led to an apparent decrease in incision upstream. Understanding these interactions is key to interpreting the exhumation rate histories of the Dazhuka-Yueju, and more importantly, the Zedong-Jiacha knickpoints.

In order to further test the normal fault control on the Pliocene-Pleistocene exhumation in the gorges, we applied forward and inverse 3D thermokinematic model using Pecube (Braun et al., 2012; Figures 5 and S3). Forward model results show good agreement between predicted and observed AHe ages in both the hanging and footwalls. In contrast, models without a normal fault cannot yield agreement between predicted and observed AHe ages in both hanging and footwalls (Figure S3b). Inverse models for free parameters indicate that (1) normal faults should be active before ca. 1.5 Ma for the Zedong-Jiacha gorge and ca. 3.1 Ma for the Dazhuka-Yueju gorge; (2) slip rates of normal faults should be ca. 3.0 mm/y for the Zedong-Jiacha gorge and 1.7 mm/y for the Dazhuka-Yueju gorge to explain the young AHe ages and thus to yield the smallest misfit (Figure 5 and S3).

7 Conclusions

We present low-temperature thermochronological ages and compile published data from both the gorge and braided valley in the main trunk and tributaries of the middle reach Yarlung River. AHe ages can be divided into two groups. First, AHe ages from braided valleys and tributaries of the Yarlung River are mainly between 9.1 Ma and 14.3 Ma. Thermal modelling reveals river-level samples from these regions underwent rapid cooling during 15-9 Ma. Given that a geothermal gradient of ~25-30 °C/km, these samples recorded a rapid exhumation from 2.8-2.0 km depth to near-surface during 15-9 Ma, and then they experienced slow exhumation rates since then. The above mid-Miocene period of rapid exhumation might be attributed to the synergistic effect of the enhanced precipitation due to the onset of Asian monsoon and extensional tectonics. Second, AHe ages of river-level samples from the gorges vary from 1.8 Ma to 5.5 Ma. Thermal histories reveal a rapid cooling during ca. 5-3 Ma in the Dazhuka-Yueju gorge and at ca. 2 Ma in the Zedong-Jiacha gorge, respectively. This stage of accelerated exhumation was limited within gorges, and it is coeval with north-south normal fault activity. Pecube modelling indicates that normal fault activity is required to explain the observed ages. Therefore, local tectonics is the first-order control on this stage of rapid exhumation.

Acknowledgments, Samples, and Data

Devon Orme, Karl Lang, Associate Editor Djordje Grujic and Editor Taylor Schildgen are greatly appreciated for their constructive comments which significantly improved this manuscript. We thank Yukui Ge and Aorigele Zhou for help in the fieldwork. This study was supported by Second Tibetan Plateau Scientific Expedition and Research Program (2019QZKK0204), National Natural Science Foundation of China (No. 41872105), Fundamental Research Funds for the Central Universities (292019062), 111 project (B18048), China Geological Survey (DD20160027). MF is supported by NERC (NE/N015479/1). DLS acknowledges the Ann and Gordon Getty Foundation and the United States National Science Foundation Continental Dynamics program (EAR-1111853). MMT received support from an NSF Graduate Research Fellowship (DGE-1106400). This is CUGB petrogeochemical

contribution PGC-201566. The data reported in this paper are available as supporting information or at the website (http://dx.doi.org/10.17632/fbv87pys7k.1).

References

Bender, A. M., R. O. Lease, L. B. Corbett, P. R. Bierman, M. W. Caffee, and T. M. Rittenour (2020), Late Cenozoic climate change paces landscape adjustments to Yukon River capture, *Nature Geoscience*, *13*(8), 571-575. https://doi.org/10.1038/ s41561-020-0611-4.

Betka, P. M., K. A. Lang, S. N. Thomson, R. Sincavage, C. Zoramthara, C. Lalremruatfela, D. Bezbaruah, P. Borgohain, L. Seeber, and M. S. Steckler (2019), Quantifying Regional Stratigraphic Correlations and Provenance from Miocene-Pliocene deposits of the Ancestral Brahmaputra Delta, a Record of Eastern Himalayan Exhumation and the Onset of the Indian Monsoon, edited, pp. T13F-0248.

Bian, S., et al. (2020), Late Pliocene onset of the Cona rift, eastern Himalaya, confirms eastward propagation of extension in Himalayan-Tibetan orogen, *Earth and Planetary Science Letters*. *544*, 116383. https://doi.org/10.1016/ j.epsl.2020.116383.

Blum, M., K. Rogers, J. Gleason, Y. Najman, J. Cruz, and L. Fox (2018), Allogenic and Autogenic Signals in the Stratigraphic Record of the Deep-Sea Bengal Fan, *Scientific Reports*, *8*(1), 7973. https://doi.org/10.1038/s41598-018-25819-5.

Bracciali, L., Y. Najman, R. R. Parrish, S. H. Akhter, and I. Millar (2015), The Brahmaputra tale of tectonics and erosion: Early Miocene river capture in the Eastern Himalaya, *Earth and Planetary Science Letters*, *415*(0), 25-37. http://dx.doi.org/10.1016/j.epsl.2015.01.022.

Braun, J., P. van der Beek, P. Valla, X. Robert, F. Herman, C. Glotzbach, V. Pedersen, C. Perry, T. Simon-Labric, and C. Prigent (2012), Quantifying rates of landscape evolution and tectonic processes by thermochronology and numerical modeling of crustal heat transport using PECUBE, *Tectonophysics*, *524–525*, 1-28. http://dx.doi.org/10.1016/j.tecto.2011.12.035.

Burg, J.-P., P. Nievergelt, F. Oberli, D. Seward, P. Davy, J.-C. Maurin, Z. Diao, and M. Meier (1998), The Namche Barwa syntaxis: evidence for exhumation related to compressional crustal folding, *Journal of Asian Earth Sciences*, 16(2-3), 239-252. http://dx.doi.org/10.1016/s0743-9547(98)00002-6.

Cao, W., J. Yang, A. V. Zuza, W.-Q. Ji, X.-X. Ma, X. Chu, and Q. P. Burgess (2020), Crustal tilting and differential exhumation of Gangdese Batholith in southern Tibet revealed by bedrock pressures, *Earth and Planetary Science Letters*, *543*, 116347. https://doi.org/10.1016/j.epsl.2020.116347.

Carrapa, B., M. Faiz bin Hassim, P. A. Kapp, P. G. DeCelles, and G. Gehrels (2017), Tectonic and erosional history of southern Tibet recorded by detrital chronological signatures along the Yarlung River drainage, *GSA Bulletin*, *129*(5-6), 570-581. https://doi.org/10.1130/B31587.1.

Carrapa, B., D. A. Orme, P. G. DeCelles, P. Kapp, M. A. Cosca, and R. Waldrip (2014), Miocene burial and exhumation of the India-Asia collision zone in southern Tibet: Response to slab dynamics and erosion, *Geology*, *42*(5), 443-446. https://doi.org/10.1130/g35350.1.

Carrapa, B., X. Robert, P. G. DeCelles, D. A. Orme, S. N. Thomson, and L. M. Schoenbohm (2016), Asymmetric exhumation of the Mount Everest region: Implications for the tectono-topographic evolution of the Himalaya, *Geology*, *44*(8), 611-614. https://doi.org/10.1130/g37756.1.

Champagnac, J.-D., P. Molnar, C. Sue, and F. Herman (2012), Tectonics, climate, and mountain topography, *Journal of Geophysical Research: Solid Earth*, *117*(B2). https://doi.org/10.1029/2011JB008348.

Chen, C., Y. Bai, X. Fang, Q. Xu, T. Zhang, T. Deng, J. He, and Q. Chen (2020), Lower-altitude of the Himalayas before the mid-Pliocene as constrained by hydrological and thermal conditions, *Earth and Planetary Science Letters, 545,* 116422. https://doi.org/10.1016/j.epsl.2020.116422.

Chirouze, F., P. Huyghe, P. van der Beek, C. Chauvel, T. Chakraborty, G. Dupont-Nivet, and M. Bernet (2013), Tectonics, exhumation, and drainage evolution of the eastern Himalaya since 13 Ma from detrital geochemistry and thermochronology, Kameng River Section, Arunachal Pradesh, *Geological Society of America Bulletin*, *125*(3-4), 523-538. https://doi.org/10.1130/b30697.1.

Cina, S. E., A. Yin, M. Grove, C. S. Dubey, D. P. Shukla, O. M. Lovera, T. K. Kelty, G. E. Gehrels, and D. A. Foster (2009), Gangdese arc detritus within the eastern Himalayan Neogene foreland basin: Implications for the Neogene evolution of the Yalu-Brahmaputra River system, *Earth and Planetary Science Letters*, *285*(1-2), 150-162. https://doi.org/10.1016/j.epsl.2009.06.005.

Clift, P. D., K. V. Hodges, D. Heslop, R. Hannigan, H. Van Long, and G. Calves (2008), Correlation of Himalayan exhumation rates and Asian monsoon intensity, *Nature Geoscience*, *1*(12), 875-880. https://doi.org/10.1038/ngeo351.

Copeland, P., T. M. Harrison, Y. Pan, W. S. F. Kidd, M. Roden, and Y. Q. Zhang (1995), Thermal evolution of the Gangdese batholith, southern Tibet: A history of episodic unroofing, *Tectonics*, *14*(2), 223-236. https://doi.org/10.1029/94tc01676.

Dai, J., C. Wang, J. Hourigan, Z. Li, and G. Zhuang (2013), Exhumation History of the Gangdese Batholith, Southern Tibetan Plateau: Evidence from Apatite and Zircon (U-Th)/He Thermochronology, *The Journal of Geology*, *121*(2), 155-172. https://doi.org/10.1086/669250.

Dai, J.-G., C.-S. Wang, R. J. Stern, K. Yang, and J. Shen (2020), Forearc magmatic evolution during subduction initiation: Insights from an Early Cretaceous Tibetan ophiolite and comparison with the Izu-Bonin-Mariana forearc, *Geological Society of America Bulletin,* https://doi.org/10.1130/b35644.1.

Decelles, P. G., P. A. Kapp, J. Quade, and G. E. Gehrels (2011), Oligocene–Miocene Kailas basin, southwestern Tibet: Record of postcollisional upper-plate extension in the Indus-Yarlung suture zone, *Geological Society of America Bulletin, 123*, 1337-1362. *https://doi.org/10.1130/B30258.1.*

Ding, L., et al. (2017), Quantifying the rise of the Himalaya orogen and implications for the South Asian monsoon, *Geology*, 45(3), 215-218. https://doi.org/10.1130/g38583.1.

Ding, L., Q. Xu, Y. Yue, H. Wang, F. Cai, and S. Li (2014), The Andean-type Gangdese Mountains: Paleoelevation record from the Paleocene–Eocene Linzhou Basin, *Earth and Planetary Science Letters*, 392(0), 250-264. http://doi.org/10.1016/j.epsl.2014.01.045.

Donelick, R. A., P. B. O'Sullivan, and R. A. Ketcham (2005), Apatite Fission-Track Analysis, *Reviews in Mineralogy and Geochemistry*, *58*(1), 49-94. https://doi.org/ 10.2138/rmg.2005.58.3.

Dunkl, I. (2002), Trackkey: a Windows program for calculation and graphical presentation of fission track data, *Computers & Geosciences*, 28(1), 3-12. https://doi.org/10.1016/S0098-3004(01)00024-3.

Farley, K. A. (2002), (U-Th)/He Dating: Techniques, Calibrations, and Applications, Noble Gas Geochemistry, *Reviews in Mineralogy and Geochemistry*, 47(1), 819-844. http://doi.org/10.2138/rmg.2002.47.18.

Finnegan, N. J., B. Hallet, D. R. Montgomery, P. K. Zeitler, J. O. Stone, A. M. Anders, and L. Yuping (2008), Coupling of rock uplift and river incision in the Namche Barwa–Gyala Peri massif, Tibet, *Geological Society of America Bulletin*, *120*(1-2), 142-155. https://doi.org/10.1130/b26224.1.

Flowers, R. M., R. A. Ketcham, D. L. Shuster, and K. A. Farley (2009), Apatite (U-Th)/He thermochronometry using a radiation damage accumulation and annealing model, *Geochimica Et Cosmochimica Acta*, *73*(8), 2347-2365. https://doi.org/ 10.1016/j.gca.2009.01.015.

Fox, M., and A. Carter (2020), Heated Topics in Thermochronology and Paths towards Resolution, *Geosciences*, 10(9), 375. https://doi.org/10.3390/geosciences10090375

Fox, M., A. Carter, and J.-G. Dai (2020), How Continuous Are the "Relict" Landscapes of Southeastern Tibet?, *Frontiers in Earth Science*, 8(522). https://doi.org/10.3389/feart.2020.587597.

Galbraith, R. F., and G. M. Laslett (1993), Statistical models for mixed fission track ages, *Nuclear Tracks and Radiation Measurements*, 21(4), 459-470. https://doi.org/10.1016/1359-0189(93)90185-c.

Gallagher, K. (2012), Transdimensional inverse thermal history modeling for quantitative thermochronology, *Journal of Geophysical Research: Solid Earth, 117*(B2), B02408. https://doi.org/10.1029/2011jb008825.

Garzione, C. N., D. L. Dettman, J. Quade, P. G. DeCelles, and R. F. Butler (2000), High times on the Tibetan Plateau: Paleoelevation of the Thakkhola graben, Nepal, *Geology, 28*(4), 339-342. https://doi.org/10.1130/0091-7613(2000)28<339:HTOTTP>2.0.CO;2.

Ge, Y., Y. Li, X. Wang, X. Qian, J. Zhang, A. Zhou, and J. Liu-Zeng (2018), Oligocene-Miocene burial and exhumation of the southernmost Gangdese mountains from sedimentary and thermochronological evidence, *Tectonophysics*, *723*, 68-80. https://doi.org/10.1016/j.tecto.2017.12.003.

Ge, Y., et al. (2020), Spatio-temporal variation in rock exhumation linked to large-scale shear zones in the southeastern Tibetan Plateau, *Science China Earth Sciences, 63*(4), 512-532. https://doi.org/10.1007/s11430-019-9567-y.

Ge, Y.-K., J.-G. Dai, C.-S. Wang, Y.-L. Li, G.-Q. Xu, and M. Danisik (2017), Cenozoic thermo-tectonic evolution of the Gangdese batholith constrained by low-temperature thermochronology, *Gondwana Research*, *41*, 451-462. http://doi.org/10.1016/j.gr.2016.05.006.

Gemignani, L., van der Beek, P. A., Braun, J., Najman, Y., Bernet, M., Garzanti, E., & Wijbrans, J. R. (2018). Downstream evolution of the thermochronologic age signal in the Brahmaputra catchment (eastern Himalaya): Implications for the detrital record of erosion. *Earth and Planetary Science Letters*, 499, 48–61. https://doi.org/10.1016/j.epsl.2018.07.019

Gourbet, L., R. Yang, M. G. Fellin, J.-L. Paquette, S. D. Willett, J. Gong, and C. Maden (2019), Evolution of the Yangtze River network, southeastern Tibet: Insights from thermochronology and sedimentology, *Lithosphere*, *12*(1), 3-18, https://doi.org/10.1130/l1104.1.

Govin, G., van der Beek, P., Najman, Y., Millar, I., Gemignani, L., Huyghe, P., et al. (2020). Early onset and late acceleration of rapid exhumation in the Namche Barwa syntaxis, eastern Himalaya. *Geology*, 48(12), 1139–1143. https://doi.org/10.1130/G47720.1.

Grujic, D., K. T. Ashley, M. A. Coble, I. Coutand, D. A. Kellett, K. P. Larson, D. M. Whipp Jr., M. Gao, and N. Whynot (2020), Deformational Temperatures Across the Lesser Himalayan Sequence in Eastern Bhutan and Their Implications for the Deformation History of the Main

Central Thrust, *Tectonics*, 39(4), e2019TC005914. https://doi.org/10.1029/2019TC005914.
Grujic, D., L. S. Hollister, and R. R. Parrish (2002), Himalayan metamorphic sequence as an orogenic channel: insight from Bhutan, *Earth and Planetary Science Letters*, 198(1–2), 177-191. http://doi.org/10.1016/S0012-821X(02)00482-X.
Harrison, T. M., P. Copeland, W. S. F. Kidd, and A. Yin (1992), Raising Tibet, *Science*, *255*(5052), 1663-1670. https://doi.org/10.1126/science.255.5052.1663.
Herman, F., D. Seward, P. G. Valla, A. Carter, B. Kohn, S. D. Willett, and T. A. Ehlers (2013), Worldwide acceleration of mountain erosion under a cooling climate, *Nature*, *504*, 423, https://doi.org/10.1038/nature12877.
Huntington, K. W., J. Saylor, J. Quade, and A. M. Hudson (2015), High late Miocene–Pliocene elevation of the Zhada Basin, southwestern Tibetan Plateau, from carbonate clumped isotope thermometry, *GSA Bulletin, 127*(1-2), 181-199. https://doi.org/10.1130/b31000.1.
Hurford, A. J., and P. F. Green (1983), The zeta age calibration of fission-track dating, *Chemical Geology*, *41*, 285-317. https://doi.org/10.1016/S0009-2541(83)80026-6.
Ingalls, M., et al. (2018), Paleocene to Pliocene low-latitude, high-elevation basins of southern Tibet: Implications for tectonic models of India-Asia collision, Cenozoic climate, and geochemical weathering, *GSA Bulletin*, *130*(1-2), 307-330. https://doi.org/10.1130/b31723.1.
Jiang, G., Hu, S., Shi, Y., Zhang, C., Wang, Z., & Hu, D. (2019). Terrestrial heat flow of continental China: Updated dataset and tectonic implications. *Tectonophysics*, *753*, 36–48. https://doi.org/10.1016/j.tecto.2019.01.006.
Kapp, P., and P. G. DeCelles (2019), Mesozoic–Cenozoic geological evolution of the Himalayan-Tibetan orogen and working tectonic hypotheses, *American Journal of Science*, 319(3), 159-254. https://doi.org/10.2475/03.2019.01.
Lang, K. A., and K. W. Huntington (2014), Antecedence of the Yarlung–Siang–Brahmaputra River, eastern Himalaya, *Earth and Planetary Science Letters*, *397*, 145-158. https://doi.org/10.1016/j.epsl.2014.04.026.
Lang, K. A., K. W. Huntington, R. Burmester, and B. Housen (2016), Rapid exhumation of the eastern Himalayan syntaxis since the late Miocene, *Geological Society of America Bulletin*, 128(9-10), 1403-1422. https://doi.org/10.1130/b31419.1.
Langille, J. M., M. J. Jessup, J. M. Cottle, G. Lederer, and T. Ahmad (2012), Timing of metamorphism, melting and exhumation of the Leo Pargil dome, northwest India, *Journal of Metamorphic Geology*, 30(8), 769-791. https://doi.org/10.1111/j.1525-1314.2012.00998.x.
Laskowski, A. K., P. Kapp, and F. Cai (2018), Gangdese culmination model: Oligocene–Miocene duplexing along the India-Asia suture zone, Lazi region, southern Tibet, *Geological Society of America Bulletin, 130*(7-8), 1355-1376. https://doi.org/10.1130/b31834.1.
Laskowski, A. K., P. Kapp, L. Ding, C. Campbell, and X. Liu (2017), Tectonic evolution of the Yarlung suture zone, Lopu Range region, southern Tibet, *Tectonics*, 36(1), 2016TC004334. https://doi.org/10.1002/2016TC004334.
Leary, R. J., P. G. DeCelles, J. Quade, G. E. Gehrels, and G. Waanders (2016), The Liuqu Conglomerate, southern Tibet: Early Miocene basin development related to deformation within the Great Counter Thrust system, *Lithosphere*, 8(5), 427-450. https://doi.org/10.1130/l542.1.
Lee, J., B. R. Hacker, W. S. Dinklage, Y. Wang, P. Gans, A. Calvert, J. Wan, W. Chen, A. E. Blythe, and W. McClelland (2000), Evolution of the Kangmar Dome, southern Tibet: Structural, petrologic, and thermochronologic constraints, *Tectonics*, *19*(5), 872-895. https://doi.org/10.1029/1999TC001147.

Lee, J., and M. J. Whitehouse (2007), Onset of mid-crustal extensional flow in southern Tibet: Evidence from U/Pb zircon ages, *Geology*, *35*(1), 45-48. https://doi.org/10.1130/G22842A.1.

Li, G., B. Kohn, M. Sandiford, and Z. Xu (2017), India-Asia convergence: Insights from burial and exhumation of the Xigaze fore-arc basin, south Tibet, *Journal of Geophysical Research: Solid Earth*, *122*(5), 2017JB014080. https://doi.org/10.1002/2017JB014080.

Li, G., B. Kohn, M. Sandiford, Z. Xu, Y. Tian, and C. Seiler (2016), Synorogenic morphotectonic evolution of the Gangdese batholith, South Tibet: Insights from low-temperature thermochronology, *Geochemistry, Geophysics, Geosystems*, *17*(1), 101-112. https://doi.org/10.1002/2015GC006047.

Li, G., Y. Tian, B. P. Kohn, M. Sandiford, Z. Xu, and Z. Cai (2015), Cenozoic low temperature cooling history of the Northern Tethyan Himalaya in Zedang, SE Tibet and its implications, *Tectonophysics*, *643*(0), 80-93. http://dx.doi.org/10.1016/j.tecto.2014.12.014.

Long, S., N. McQuarrie, T. Tobgay, and D. Grujic (2011), Geometry and crustal shortening of the Himalayan fold-thrust belt, eastern and central Bhutan, *Geological Society of America Bulletin*, 123(7-8), 1427-1447. http://dx.doi.org/10.1130/b30203.1.

Montgomery, D. R., and M. T. Brandon (2002), Topographic controls on erosion rates in tectonically active mountain ranges, *Earth and Planetary Science Letters*, *201*(3–4), 481-489. https://doi.org/10.1016/s0012-821x(02)00725-2.

Nie, J., et al. (2018), Rapid incision of the Mekong River in the middle Miocene linked to monsoonal precipitation, *Nature Geoscience*, *11*(12), 944-948. https://doi.org/10.1038/s41561-018-0244-z.

Orme, D. A. (2019), Burial and exhumation history of the Xigaze forearc basin, Yarlung suture zone, Tibet, *Geoscience Frontiers*, *10*(3), 895-908. https://doi.org/10.1016/j.gsf.2017.11.011.

Orme, D. A., B. Carrapa, and P. Kapp (2015), Sedimentology, provenance and geochronology of the upper Cretaceous–lower Eocene western Xigaze forearc basin, southern Tibet, *Basin Research, 27*(4), 387-411. https://doi.org/10.1111/bre.12080.

Orme, D. A., and A. K. Laskowski (2016), Basin Analysis of the Albian–Santonian Xigaze Forearc, Lazi Region, South-Central Tibet, *Journal of Sedimentary Research*, 86(8), 894-913. https://doi.org/10.2110/jsr.2016.59.

Ouimet, W., K. Whipple, L. Royden, P. Reiners, K. Hodges, and M. Pringle (2010), Regional incision of the eastern margin of the Tibetan Plateau, *Lithosphere*, *2*(1), 50-63. https://doi.org/10.1130/l57.1.

Pan, G., J. Ding, D. Yao, L. Wang, and compilers. (2004), Guidebook of 1:1,500,000 geologic map of the Qinghai-Xizang (Tibet) plateau and adjacent areas, Chengdu, China, Chengdu Cartographic Publishing House, 48 p.

Pan, Y., and W. Kidd (1992), Nyainqentanglha shear zone; a late Miocene extensional detachment in the southern Tibetan Plateau, *Geology*, *20*(9), 775-778. https://doi.org/10.1130/0091-7613(1992)020<0775:NSZALM>2.3.CO;2.

Quade, J., D. O. Breecker, M. Daeron, and J. Eiler (2011), The paleoaltimetry of Tibet: An isotopic perspective, *American Journal of Science*, 311(2), 77-115. https://doi.org/ 10.2475/02.2011.01.

Replumaz, A., et al. (2020), Tectonic Control on Rapid Late Miocene—Quaternary Incision of the Mekong River Knickzone, Southeast Tibetan Plateau, *Tectonics*, *39*(2), e2019TC005782. https://doi.org/10.1029/2019tc005782.

Robinson, R. A. J., C. A. Brezina, R. R. Parrish, M. S. A. Horstwood, O. Nay Win, M. I. Bird, T. Myint, A. S. Walters, G. J. H. Oliver, and Z. Khin (2014), Large rivers and orogens: The

evolution of the Yarlung Tsangpo–Irrawaddy system and the eastern Himalayan syntaxis, *Gondwana Research*, *26*(1), 112-121. http://dx.doi.org/10.1016/j.gr.2013.07.002.

Rohrmann, A., P. Kapp, B. Carrapa, P. W. Reiners, J. Guynn, L. Ding, and M. Heizler (2012), Thermochronologic evidence for plateau formation in central Tibet by 45 Ma, *Geology*, *40*(2), 187-190. https://doi.org/10.1130/g32530.1.

Rowley, D. B., T. Pierrehumbert, and C. B. S. (2001), A new approach to stable isotope-based paleoaltimetry: implications for paleoaltimetry and paleohypsometry of the High Himalaya since the Late Miocene, *Earth and Planetary Science Letters, 188*, 253-268. https://doi.org/10.1016/S0012-821X(01)00324-7.

Schildgen, T. F., G. Balco, and D. L. Shuster (2010), Canyon incision and knickpoint propagation recorded by apatite He-4/He-3 thermochronometry, *Earth and Planetary Science Letters*, 293(3-4), 377-387. https://doi.org/10.1016/j.epsl.2010.03.009.

Schildgen, T. F., K. V. Hodges, K. X. Whipple, P. W. Reiners, and M. S. Pringle (2007), Uplift of the western margin of the Andean plateau revealed from canyon incision history, southern Peru, *Geology*, *35*(6), 523-526. https://doi.org/10.1130/G23532A.1.

Schildgen, T. F., P. A. van der Beek, H. D. Sinclair, and R. C. Thiede (2018), Spatial correlation bias in late-Cenozoic erosion histories derived from thermochronology, *Nature*, *559*(7712), 89-93. https://doi.org/10.1038/s41586-018-0260-6.

Schmidt, J. L., P. K. Zeitler, F. J. Pazzaglia, M. M. Tremblay, D. L. Shuster, and M. Fox (2015), Knickpoint evolution on the Yarlung river: Evidence for late Cenozoic uplift of the southeastern Tibetan plateau margin, *Earth and Planetary Science Letters*, *430*, 448-457. http://dx.doi.org/10.1016/j.epsl.2015.08.041.

Seward, D., and J.-P. Burg (2008), Growth of the Namche Barwa Syntaxis and associated evolution of the Tsangpo Gorge: Constraints from structural and thermochronological data, *Tectonophysics*, *451*(1–4), 282-289. https://doi.org/10.1016/j.tecto.2007.11.057.

Shuster, D. L., K. M. Cuffey, J. W. Sanders, and G. Balco (2011), Thermochronometry Reveals Headward Propagation of Erosion in an Alpine Landscape, *Science*, *332*(6025), 84-88. https://doi.org/10.1126/science.1198401.

Styron, R. H., M. H. Taylor, K. E. Sundell, D. F. Stockli, J. A. G. Oalmann, A. Möller, A. T. McCallister, D. Liu, and L. Ding (2013), Miocene initiation and acceleration of extension in the South Lunggar rift, western Tibet: Evolution of an active detachment system from structural mapping and (U-Th)/He thermochronology, Tectonics, 32(4), 880-907. https://doi.org/10.1002/tect.20053.

Sundell, K. E., M. H. Taylor, R. H. Styron, D. F. Stockli, P. Kapp, C. Hager, D. Liu, and L. Ding (2013), Evidence for constriction and Pliocene acceleration of east-west extension in the North Lunggar rift region of west central Tibet, Tectonics, 32(5), 1454-1479. https://doi.org/10.1002/tect.20086.

Tremblay, M. M., M. Fox, J. L. Schmidt, A. Tripathy-Lang, M. M. Wielicki, T. M. Harrison, P. K. Zeitler, and D. L. Shuster (2015), Erosion in southern Tibet shut down at ∼10 Ma due to enhanced rock uplift within the Himalaya, *Proceedings of the National Academy of Sciences*, *112*(39), 12030-12035. https://doi.org/10.1073/pnas.1515652112.

Tu, J.-Y., J.-Q. Ji, D.-X. Sun, J.-F. Gong, D.-L. Zhong, and B.-F. Han (2015), Thermal structure, rock exhumation, and glacial erosion of the Namche Barwa Peak, constraints from thermochronological data, *Journal of Asian Earth Sciences*, *105*, 223-233. https://doi.org/10.1016/j.jseaes.2015.03.035.

Wang, C., J. Dai, X. Zhao, Y. Li, S. A. Graham, D. He, B. Ran, and J. Meng (2014a), Outward-

growth of the Tibetan Plateau during the Cenozoic: A review, *Tectonophysics*, 621(0), 1-43. http://dx.doi.org/10.1016/j.tecto.2014.01.036.

Wang, P., D. Scherler, J. Liu-Zeng, J. Mey, J.-P. Avouac, Y. Zhang, and D. Shi (2014b), Tectonic control of Yarlung Tsangpo Gorge revealed by a buried canyon in Southern Tibet, *Science*, *346*(6212), 978-981. https://doi.org/ 10.1126/science.1259041.

Wang, Y., X. Zhang, L. Sun, and J. Wan (2007), Cooling history and tectonic exhumation stages of the south-central Tibetan Plateau (China): Constrained by 40Ar/39Ar and apatite fission track thermochronology, *Journal of Asian Earth Sciences*, *29*(2-3), 266-282. https://doi.org/10.1016/j.jseaes.2005.11.001.

Webb, A. A. G., H. Guo, P. D. Clift, L. Husson, T. Müller, D. Costantino, A. Yin, Z. Xu, H. Cao, and Q. Wang (2017), The Himalaya in 3D: Slab dynamics controlled mountain building and monsoon intensification, *Lithosphere, 9*(4), 637-651. https://doi.org/10.1130/l636.1.

Whipple, K. X. (2004), Bedrock rivers and the geomorphology of active orogens, *Annual Review of Earth and Planetary Sciences*, *32*, 151-185. https://doi.org/10.1146/annurev.earth.32.101802.120356.

Willett, S. D., Herman, F., Fox, M., Stalder, N., Ehlers, T. A., Jiao, R., & Yang, R. (2020). Bias and error in modelling thermochronometric data: resolving a potential increase in Plio-Pleistocene erosion rate. *Earth Surface Dynamics* Discussions, 1–78. https://doi.org/10.5194/esurf-2020-59.

Wolff, R., R. Hetzel, I. Dunkl, Q. Xu, M. Bröcker, and A. A. Anczkiewicz (2019), High-Angle Normal Faulting at the Tangra Yumco Graben (Southern Tibet) since ~15 Ma, *The Journal of Geology*, 127(1), 15-36. https://doi.org/10.1086/700406.

Yang, R., F. Herman, M. G. Fellin, and C. Maden (2018), Exhumation and topographic evolution of the Namche Barwa Syntaxis, eastern Himalaya, *Tectonophysics*, *722*, 43-52. https://doi.org/10.1016/j.tecto.2017.10.026.

Yin, A. (2006), Cenozoic tectonic evolution of the Himalayan orogen as constrained by along-strike variation of structural geometry, exhumation history, and foreland sedimentation, *Earth-Science Reviews*, *76*(1-2), 1-131. https://doi.org/ 10.1016/j.earscirev.2005.05.004.

Yin, A., T. Harrison, F. Ryerson, W. Chen, W. Kidd, and P. Copeland (1994), Tertiary structural evolution of the Gangdese thrust system, southeastern Tibet, *Journal of Geophysical Research*, *99*(B9), 18175-18201. https://doi.org/10.1029/94JB00504.

Yu, X., J. Ji, J. Gong, D. Sun, J. Qing, L. Wang, D. Zhong, and Z. Zhang (2011), Evidences of rapid erosion driven by climate in the Yarlung Zangbo (Tsangpo) Great Canyon, the eastern Himalayan syntaxis, *Chinese Science Bulletin*, *56*(11), 1123-1130. https://doi.org/10.1007/s11434-011-4419-x.

Yuan, W., J. Deng, Q. Zheng, J. Dong, Z. Bao, P. R. Eizenhoefer, X. Xu, and Z. Huang (2009), Apatite fission track constraints on the Neogene tectono-thermal history of Nimu area, southern Gangdese terrane, Tibet Plateau, *Island Arc*, *18*(3), 488-495. https://doi.org/10.1111/j.1440-1738.2009.00669.x.

Yuan, W., S. Wang, S. Li, and Z. Yang (2002), Apatite fission track dating evidence on the tectonization of Gangdese block, south Qinghai-Tibetan Plateau, *Chinese Science Bulletin*, *47*(3), 240-244. https://doi.org/10.1360/02tb9057.

Zachos, J., M. Pagani, L. Sloan, E. Thomas, and K. J. s. Billups (2001), Trends, rhythms, and aberrations in global climate 65 Ma to present, *292*(5517), 686-693. https://doi.org/ 10.1126/science.1059412.

Zeitler, P. K., A. S. Meltzer, L. Brown, W. S. F. Kidd, C. Lim, and E. Enkelmann (2014), Tectonics

and topographic evolution of Namche Barwa and the easternmost Lhasa block, Tibet, *Geological Society of America Special Papers*, *507*, 23-58. https://doi.org/10.1130/2014.2507(02).

Zeitler, P. K., A. S. Meltzer, P. O. Koons, D. Craw, B. Hallet, C. P. Chamberlain, W. S. F. Kidd, S. K. Park, L. Seeber, and M. Bishop (2001), Erosion, Himalayan geodynamics, and the geomorphology of metamorphism, *GSA Today*, *11*(1), 4-9.

Zhang, D. D. (1998), Geomorphological problems of the middle reaches of the Tsangpo River, Tibet, *Earth Surface Processes and Landforms*, *23*(10), 889-903. https://doi.org/10.1002/(SICI)1096-9837(199810)23:10<889::AID-ESP907>3.0.CO;2-E.

Zhang, J.-Y., A. Yin, W.-C. Liu, L. Ding, and X.-M. Xu (2016), First geomorphological and sedimentological evidence for the combined tectonic and climate control on Quaternary Yarlung river diversion in the eastern Himalaya, *Lithosphere*, *8*(3), 293-316. https://doi.org/10.1130/l500.1.

Zhang, P., et al. (2019), Palaeodrainage evolution of the large rivers of East Asia, and Himalayan-Tibet tectonics, *Earth-Science Reviews*, 192, 601-630. https://doi.org/10.1016/ j.earscirev.2019.02.003.

Zhang, P. Z., P. Molnar, and W. R. Downs (2001), Increased sedimentation rates and grain sizes 2–4 Myr ago due to the influence of climate change on erosion rates, *Nature*, *410*, 891. https://doi.org/10.1038/35073504.

Zhu, D.-C., Z.-D. Zhao, Y. Niu, X.-X. Mo, S.-L. Chung, Z.-Q. Hou, L.-Q. Wang, and F.-Y. Wu (2011), The Lhasa Terrane: Record of a microcontinent and its histories of drift and growth, *Earth and Planetary Science Letters*, 301(1–2), 241-255. https://doi.org/10.1016/j.epsl.2010.11.005.